

This paper is a non-peer reviewed preprint submitted to EarthArXiv. This paper has been submitted to ESA Ecological Applications. Copyright in this Work may be transferred without further notice.

A Bayesian Approach to Hyperspectral Leaf Trait Prediction with uncertainty quantification

Dhruva Kathuria^{1,2}, Yoseline Angel^{1,3}, Evan Lang^{1,3}, Alexey N. Shiklomanov¹

¹ NASA Goddard Space Flight Center, Greenbelt, Maryland, USA

² GESTAR II, Morgan State University, Baltimore, Maryland, USA

³ ESSIC, University of Maryland, College Park, Maryland, USA

⁴ Science Systems and Applications, Inc. (SSAI), Lanham, Maryland, USA

Corresponding author: Dhruva Kathuria, NASA Goddard Space Flight Center, Greenbelt, Maryland, USA; GESTAR II, Morgan State University, Baltimore, Maryland, USA. Email: dhruva.kathuria@nasa.gov

Open Research Statement

Ecosis data used in this study is freely available at <https://ecosis.org>. The codes used in this study are available at https://github.com/DhruvaKathuria/Hierarchical_foliar_trait_estimation.

Example datasets are available at <https://zenodo.org/records/19614757>.

Keywords

Bayesian, dimension reduction, hyperspectral reflectance, Partial Least Squares Regression, plant functional traits, trait-spectra relationship, uncertainty quantification

1 Abstract

2 Leaf functional traits are leaf features that determine ecosystem functioning, plant growth, and
3 resource allocation. Most traits can be derived from leaf reflectance measurements across the
4 visible to shortwave infrared range using empirical and physical methods. Partial Least Squares
5 Regression (PLSR) is widely used but has limitations in uncertainty quantification and model
6 flexibility. In this study, we present a Bayesian approach for predicting leaf traits from reflectance
7 data (400–2400 nm at 1 nm resolution) that addresses these limitations. The method eliminates
8 spectral transformation while enabling rigorous uncertainty quantification. We apply it to predict
9 carotenoid content (Car_A), nitrogen percentage mass (N_M), and Leaf Mass per Area (LMA). On an
10 independent validation dataset, the Bayesian approach performs comparably to PLSR with added
11 flexibility and robust uncertainty quantification. To enhance computational efficiency, we project
12 the full model to a reduced model using selected wavelengths (14 for Car_A , 28 for N_M , and 30 for
13 LMA), maintaining predictive performance while enabling faster predictions and trait-specific
14 wavelength insights. The Bayesian method is highly adaptable, supporting future development of
15 nonlinear, hierarchical, and multivariate models with rigorous uncertainty quantification.

16 2 Introduction

17 Leaf functional traits are measurable morphological, anatomical, physiological, biochemical, and
18 phenological features that characterize plant species functioning, their environmental responses,
19 and adaptation to changes (Lavorel and Garnier 2002; Wright et al. 2005; Violle et al. 2007). As
20 plants' primary photosynthetic organs, leaves drive the dynamic of terrestrial ecosystems. As a
21 result, leaf traits are used as input parameters in global ecosystem models to account for
22 photosynthetic capacity, plant growth, and biogeochemical cycles, and uncertainty and variability
23 in leaf traits are major sources of uncertainty in model predictions of ecosystem composition and
24 function (Wullschleger et al. 2014; Friedlingstein et al. 2006; Shiklomanov, Bond-Lamberty, et
25 al. 2020). The National Academy of Sciences 2017 Decadal Survey specifically identifies the

26 spatio-temporal distribution of plant functional traits as a crucial objective (E-1a). Plant
27 functional traits are also identified as an Essential Biodiversity Variable (Pereira et al. 2013;
28 Pettorelli et al. 2016).

29 Many leaf traits can be estimated from leaf spectral measurements in the visible to shortwave
30 infrared (VSWIR) range (~350–2500 nm) using either empirical or physically-based estimation
31 methods (Jacquemoud and Ustin 2019; Angel and Shiklomanov 2022). To date, the empirical
32 approach has been the dominant method of predicting traits using spectra due to (a) ease of
33 application, (b) computational efficiency, and (c) ability to be applied to a wide range of traits
34 (Wang et al. 2019). Among empirical methods, Partial Least Squares Regression (PLSR) (Wold
35 et al. 1984), Random Forest (Pullanagari, Kereszturi, and Yule 2016), Neural Networks (Cherif et
36 al. 2023), and Gaussian Process Regression (Wang et al. 2019) have shown considerable promise.
37 Of these approaches, only Gaussian Process Regression allows rigorous uncertainty
38 quantification, but it is computationally expensive.

39 PLSR remains the most widely used empirical approach for predicting a wide variety of traits
40 (Verrelst et al. 2019; Hansen and Schjoerring 2003; Serbin et al. 2019) due to its ease of use,
41 computational efficiency, and ability to handle predictor collinearity. This is because PLSR
42 transforms the input predictors (in this case, reflectance at individual spectral bands) into a handful
43 of orthogonal latent components. As a result, it can be applied even when the number of predictors
44 is greater than the number of training observations. However, the PLSR approach comes with its
45 own set of shortcomings. PLSR is prone to overfitting, necessitating the need of using
46 computationally expensive ways—such as minimizing the cross-validation prediction residual
47 sum of squares (PRESS) statistic (Allen 1971)—to determine the number of latent components.
48 In some cases, the PLSR method can still overfit, necessitating the need to set a threshold on the
49 number of PLSR components. PLSR is highly sensitive to outliers even if the number of outliers
50 is small compared to the total number of observations (Burnett et al. 2021). Additionally, the
51 PLSR approach to trait estimation does not provide rigorous uncertainty estimates but instead
52 relies on resampling strategies (such as bootstrapping), which can lead to inaccurate confidence
53 intervals for small to medium datasets (Chernick and Labudde 2009; Hesterberg 2015). It is also

54 difficult to extend the PLSR approach to account for hierarchical multivariate relationships that
55 might exist in certain traits (Shiklomanov, Cowdery, et al. 2020); consequently, it is challenged by
56 the variability of the relationship between traits and spectra across species, functional types, and
57 biomes. This limitation can be especially pronounced for under-sampled species.

58 To account for certain shortcomings of PLSR (and other empirical approaches), Bayesian
59 regression methods offer an attractive alternative. Bayesian methods provide robust uncertainty
60 quantification, can integrate with physical models (e.g., O’Hagan and West 2013), and
61 accommodate measurement errors from various instruments (Gustafson 2003). They are readily
62 adaptable to more complex models, such as hierarchical Bayesian models (Shiklomanov,
63 Cowdery, et al. 2020), which can account for site-specific and group-specific effects (e.g., at the
64 plant functional type or species level). Bayesian statistical methods have also been successfully
65 employed to combine multi-sensor measurements across spatial and temporal domains for
66 different environmental applications (Gelfand, Zhu, and Carlin 2001; Kathuria, Mohanty, and
67 Katzfuss 2019). Furthermore, Bayesian methods can incorporate information from secondary
68 sources and expert opinions, in the form of prior distributions. This capability makes them
69 valuable tools in the recent push for hybrid physical-empirical trait estimation approaches (Berger
70 et al. 2020).

71 The objective of this paper is to present a computationally efficient Bayesian regression framework
72 that estimates traits directly from reflectance spectra (without any latent transformation) while
73 rigorously propagating uncertainties. To achieve this, we employ a special class of shrinkage
74 priors that enable us to use Bayesian regression with high-dimensional, correlated hyperspectral
75 data while preventing overfitting. To enhance the computational efficiency of the Bayesian
76 algorithm, we apply a predictive projection technique (Piironen, Paasiniemi, and Vehtari 2020)
77 that projects the full Bayesian model onto a reduced model with a small subset of input
78 wavelengths while preserving predictive accuracy. This technique is distinctive in that the
79 selection of relevant wavelengths is based on predictions arising from the Bayesian model (which
80 accounts for measurement error) rather than directly using the noisy trait observations for variable
81 selection. Past studies have demonstrated that even when the true error structure of the data is

82 unknown, model reduction techniques such as the one described outperform variable selection
83 methods directly applied to (noisy) observations (Piiironen and Vehtari 2017b). We also discuss
84 how the Bayesian framework can be easily extended to complex models such as hierarchical,
85 multivariate, and non-linear models, which will potentially open a previously unexplored research
86 territory of exploring novel relationships between spectra and traits.

87 **3 Materials and Methods**

88 **3.1 Study Area and Data**

89 To assess the feasibility of the proposed method, we use paired observations of leaf reflectance
90 spectra spanning wavelengths from 400 to 2400 nm and three important leaf traits: carotenoid
91 content per unit area (Car_A), nitrogen mass fraction (N_M), and leaf mass per area (LMA).
92 Carotenoids are leaf pigments crucial for photosynthesis, photooxidative protection,
93 pigmentation, and phytohormone synthesis (Armstrong and Hearst 1996; Sun et al. 2022).
94 Carotenoid-derived compounds affect the flavor and aroma of crops, as well as the development of
95 defense-related plant compounds (Simkin 2021). Leaf nitrogen is related to plant photosynthetic
96 rate—most importantly through ribulose-1,5-bisphosphate carboxylase/oxygenase
97 (Rubisco)—and is useful for parameterizing photosynthetic processes in ecosystem models
98 (Onoda et al. 2017; Evans and Clarke 2019). LMA is defined as the ratio of oven-dry mass (g) to
99 the area of one side of a fresh leaf (Jacquemoud and Ustin 2019), and it is correlated with leaf
100 longevity (Osnas et al. 2013), decomposition rate (Cornelissen and Thompson 1997), and
101 photosynthetic and respiratory rates (Oren et al. 1986).
102 We obtained these data from the publicly available Ecological Spectral Information System
103 (EcoSIS) library (<https://ecosis.org>). We took only those data which have all the reflectance
104 spectral wavelengths available from 400 to 2400 nm at a spectral sampling of 1 nm in 2001
105 continuous bands. Since the trait units are different across study areas, the traits are converted to
106 common units; Car_A : $\mu\text{g cm}^{-2}$, N_M : (mg g^{-1}) and LMA : g m^{-2} . The observations used for
107 training the models span a wide range of climatic zones and biomes (Figure 1). The three traits

108 were also chosen because the number of training observations varies significantly across the three
109 traits (Car_A : 394, N_M : 541, LMA: 5,934), which helps demonstrate the algorithm’s accuracy
110 across different training set sizes.

111 To validate the algorithms, we hold out data collected as part of the Canadian Airborne
112 Biodiversity Observatory (CABO; Kothari et al. (2023)) from 2018-2019. The CABO dataset is
113 chosen as test data as it represents a comprehensive number of observations for all the analyzed
114 traits (Car_A : 1764, N_M : 1746, LMA: 1792) across a wide variety of plant growth forms:
115 broadleaf trees (~ 51.3%), graminoids (~ 18.0%), forbs (~ 12.5%), shrubs (~ 10.6%), conifer
116 trees (~ 6.5%), vines (~ 0.8%), and ferns (~ 0.3%). The CABO dataset was primarily collected in
117 Eastern Canada, with the rest of the dataset collected in Western Canada and Australia. All the
118 CABO study sites depicted in Figure 1 measure all three traits.

119 **3.2 Model description**

120 In this section, we first describe the Bayesian regression models used in predicting leaf traits using
121 hyperspectral data. Notationally, we denote a scalar with a lower case letter, a vector with bold
122 lower case letter, and a matrix with an upper case letter. Superscript T refers to transpose. All
123 vectors are assumed to be column vectors.

124 **3.2.1 Full Bayesian regression model**

125 Let the trait to be predicted be defined as a random variable y . For an i^{th} observation, let the
126 measured trait value be defined as y_i and the corresponding input spectral predictors plus intercept
127 be defined as the vector $\mathbf{x}_i = (1, x_{i,400}, x_{i,401}, \dots, x_{i,2399}, x_{i,2400})$. We assume that y has a Gaussian
128 distribution such that the mean of the distribution $\mu(x) = E(y|x)$ is a linear function of x with
129 independent and identically distributed error having constant variance σ^2 :

$$\begin{aligned} y_i &= \mu(x_i) + \epsilon_i \\ &= \boldsymbol{\beta}^T \mathbf{x}_i + \epsilon_i, \epsilon \sim N(0, \sigma^2), i = 1, \dots, n \end{aligned} \tag{1}$$

130 Here, $\boldsymbol{\beta}$ denotes the vector of corresponding regression coefficients for \mathbf{x}_i , n is the number of

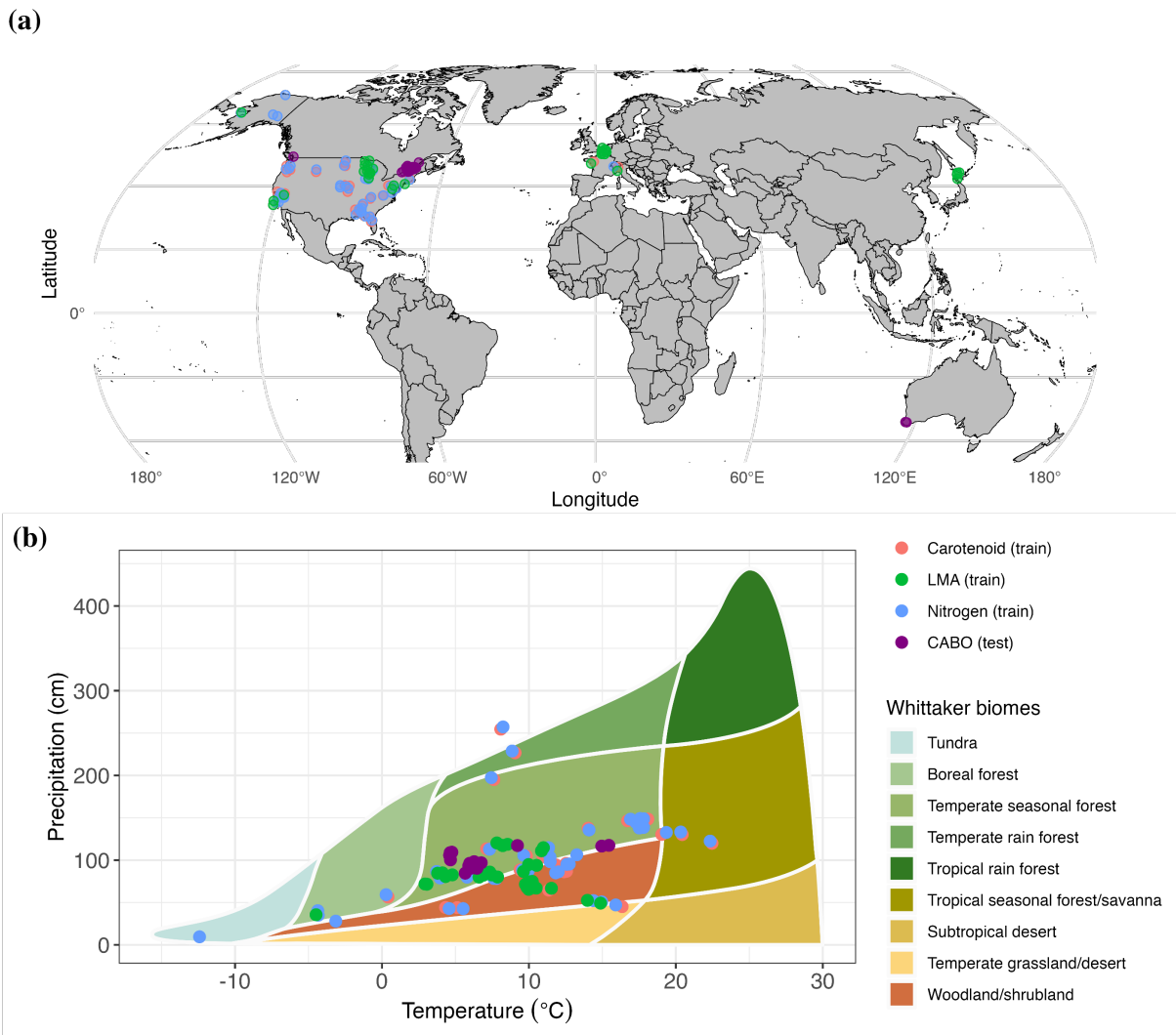


Figure 1: (a) Locations of the study sites for each of the three traits. The training datasets span diverse global locations for carotenoid (orange), leaf mass per area (green), and nitrogen (blue). The test dataset, used to validate the algorithms comprise measurements collected as part of the Canadian Airborne Biodiversity Observatory (CABO). The CABO data (purple) include observations for all three traits. (b) Whittaker biomes denoting the variation of biome range for the analyzed datasets.

131 observations, and the length of \mathbf{x}_i is the number of input wavelengths (denoted by $l = 2001$), plus
132 intercept. We can also write Equation 1 as a multivariate normal distribution of size n :

$$p(\mathbf{y}|\boldsymbol{\beta}, \sigma^2) = p(\mathbf{y}|\boldsymbol{\theta}) = N_n(\mu(X), \sigma^2 I) = N_n(X\boldsymbol{\beta}, \sigma^2 I) \quad (2)$$

133 where $\mathbf{y} = (y_1, y_2, \dots, y_n)$ is a vector of n leaf trait observations, $\boldsymbol{\theta} := (\boldsymbol{\beta}, \sigma^2)$ represent the
134 parameters of the model, X is the corresponding $n \times (l + 1)$ matrix of input bands, and I is an
135 identity matrix of size n . Let the training data for the regression model (i.e., n paired observations
136 of trait and spectra) be denoted by \mathcal{D} .

137 3.2.1.1 Formulating priors

138 An important component of the Bayesian approach is to formulate appropriate priors for the
139 parameter vector $\boldsymbol{\theta}$ used in the model. A prior distribution represents our belief about these
140 parameters and their uncertainty before observing the training data \mathcal{D} . In this work, we start with
141 the prior belief that a trait is sensitive only to a subset of the wavelengths. This prior belief makes
142 sense because leaf functional traits are sensitive to particular wavelengths in the VSWIR region.
143 Additionally, given the large dimensionality of $\boldsymbol{\beta}$ and (generally) low number of observations for a
144 given trait, using the traditional normally distributed priors for $\boldsymbol{\beta}$ can lead to overfitting of the
145 Bayesian model. This is especially true when the number of observations in \mathcal{D} is less than or
146 comparable to l .

147 Since a given trait is assumed to be sensitive to a subset of the wavelengths, we need a prior
148 distribution that shrinks the $\boldsymbol{\beta}$ coefficients of the non-important wavelengths (with respect to the
149 analyzed trait) to zero while letting the regression coefficients of the important wavelengths escape
150 this shrinkage. Such a prior distribution should therefore assign a high probability density at zero
151 while also have a heavy-tail (i.e., have non-trivial probabilities for large values of $\boldsymbol{\beta}$, which allows
152 modeling of large values of $\boldsymbol{\beta}$) for important wavelengths. To achieve this, we use the regularized
153 horseshoe prior distribution (Pironen and Vehtari 2017a), which is an extension of the original
154 horseshoe prior (Carvalho, Polson, and Scott 2010) widely used in high-dimensional regression,
155 given its theoretical properties and practical applications (Datta and Ghosh 2013; Erp, Oberski,

156 and Mulder 2019). For j^{th} regression coefficient β_j , the regularized horseshoe prior is defined as:

$$\begin{aligned}
 \beta_j &\sim N(0, \tau^2 \tilde{\lambda}_j^2) \\
 \tau^2 &\sim C^+(0, \tau_0^2), \\
 \tilde{\lambda}_j^2 &= \frac{c^2 \lambda_j^2}{c^2 + \tau^2 \lambda_j^2} \\
 \tau_0^2 &= \frac{l_0}{l - l_0} \sigma \\
 \lambda_j &\sim C^+(0, 1) \text{ for } j = 1, \dots, l \\
 c^2 &\sim IG(\nu/2, \nu s^2/2)
 \end{aligned} \tag{3}$$

157 The τ^2 parameter in regularized horseshoe prior –modeled as a standard half-Cauchy distribution
 158 on the positive reals (C^+) with scale parameter τ_0^2 – can be considered as a global shrinkage
 159 parameter which drives all regression coefficients to zero. The closer τ_0^2 gets to zero, the larger is
 160 the global shrinkage resulting from τ^2 . The parameter τ_0^2 is a function of l_0 which is defined as
 161 our guess about the number of important bands for predicting a trait. For our analysis, we set $\frac{l_0}{l-l_0}$
 162 as 0.025 for all the traits, denoting our *a priori* guess that l_0 is approximately equal to 50 bands (as
 163 $l = 2001$). Though better *a priori* guesses for individual traits can be set by consulting past
 164 literature, we avoid it to maintain generality of the proposed approach. Moreover, regularized
 165 horseshoe prior has been shown to perform well even with a crude guess for the number of
 166 relevant predictors (Piironen and Vehtari 2017a).

167 The parameter $\tilde{\lambda}_j$ —unique for each regression coefficient—is a local shrinkage parameter that
 168 allows a regression coefficient to escape this shrinkage towards zero (by having a large $\tilde{\lambda}_j$ value).
 169 The parameter $\tilde{\lambda}_j$ is a function of τ^2 , λ_j and c . The parameter λ_j is modeled as having a C^+
 170 distribution with a scale parameter of 1 resulting in heavy-right tails which allows the important
 171 wavelengths to escape shrinkage introduced by τ_0^2 . The parameter c further improves the
 172 shrinkage capabilities of the regularized horseshoe prior over the original horseshoe and is
 173 assumed to have an Inverse-Gamma (*IG*) distribution with parameters ν and s . We fix $\nu = 4$ and
 174 $s = 2$ following Piironen and Vehtari (2017a). The regularized horseshoe performs better than the
 175 original horseshoe especially when the regression coefficients are weakly identified (which can

176 happen if the input wavelengths are highly correlated) and has better sampling robustness using
 177 Markov Chain Monte Carlo (MCMC) methods (Piironen and Vehtari 2017a). Note that the
 178 regularized horseshoe prior does not make the shrunk β coefficients exactly zero, but “pulls” them
 179 towards zero.

180 Figure 2 gives the comparison between the probability density histograms of the regularized
 181 horseshoe prior and the Gaussian prior by simulating 5000000 samples for a regression coefficient
 182 β_j following Equation 3 and from a Gaussian distribution with mean 0 and standard deviation
 183 0.05. The horseshoe prior assigns a significantly higher probability at zero leading to better
 184 shrinkage of regression coefficients towards zero for non-important wavelengths. It also has a
 185 heavier tail than the Gaussian distribution allowing larger values for the beta coefficients for
 186 important wavelengths. For the intercept term in β and the error variance σ^2 in the model, we use
 187 an improper flat prior in the brms package (Bürkner 2017) denoting non-informative priors. We
 188 standardize the input wavelengths to have a mean of 0 and a standard deviation of 1.

189 3.2.1.2 Parameter estimation

190 Bayesian inference consists of getting posterior probability distribution of the parameters of the
 191 Bayesian model—as opposed to point estimates given by non-Bayesian methods such as
 192 PLSR—denoting how our belief in the parameter distribution changes (with respect to the prior
 193 distribution) after we account for the training data \mathcal{D} . Assuming that the prior distribution of the
 194 parameters are independent from each other, the posterior parameter distribution is denoted by:

$$\begin{aligned}
 p(\beta, \sigma^2 | \mathbf{y}) &\propto p(\mathbf{y} | \beta, \sigma^2) p(\beta, \sigma^2) \\
 &= p(\mathbf{y} | \beta, \sigma^2) p(\sigma^2) \prod_{j=1}^l p(\beta_j)
 \end{aligned}
 \tag{4}$$

195 where $p(\mathbf{y} | \beta, \sigma^2)$ is given by Equation 2. For computing the posterior probability distribution, we
 196 use the probabilistic programming language Stan (Stan Development Team 2018) which uses
 197 Markov chain Monte Carlo (MCMC) algorithms such as the Hamiltonian Monte Carlo (HMC)
 198 (Duane et al. 1987) and its extension the No-U-Turn Sampler (NUTS) (Hoffman and Gelman

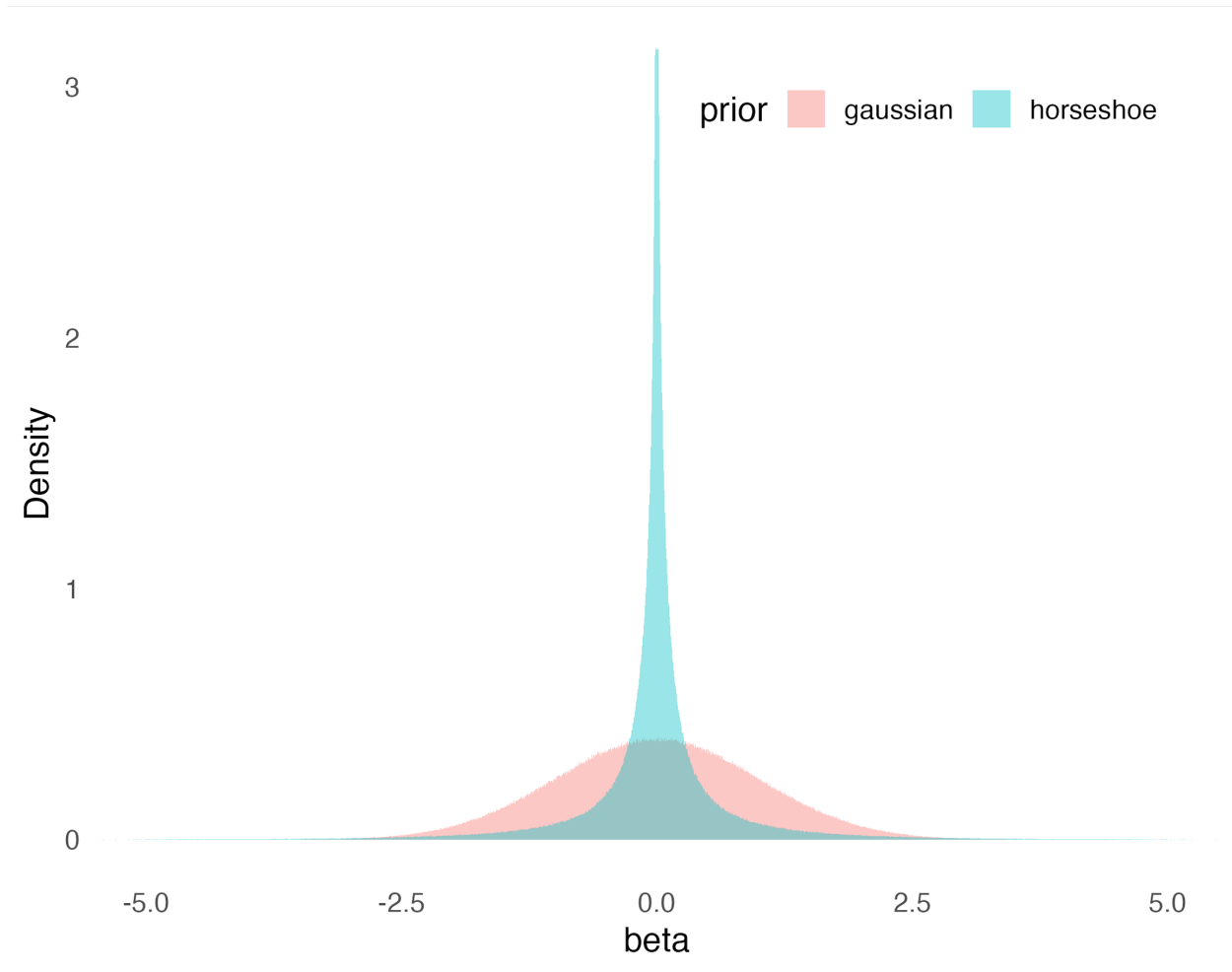


Figure 2: Probability density histograms of the Gaussian prior and Regularized horseshoe prior (binwidth = 0.003, y-axis normalized so that the area under each histogram sums to 1). The y-axis is truncated at 3 for visual clarity, as the horseshoe prior places a high probability density near zero. Compared to the normal prior, the horseshoe prior has more probability on zero for better shrinkage of non-important wavelengths towards zero and has heavier tails to allow the regression coefficients to take larger values for important wavelengths.

199 2014). These algorithms work well with high dimensional models and can be used with any prior
200 distribution (Hoffman and Gelman 2014; Betancourt 2017; Bürkner 2017). The Stan
201 implementation is done using the R language interface provided by the package brms (Bürkner
202 2017).

203 We ran three MCMC chains in parallel, each for 50,000 iterations (after a warm-up of 10,000
204 iterations), thinned at an interval of 10 iterations resulting in a total of 15,000 MCMC samples.
205 To assess the convergence of the parameters in the MCMC chain, we confirmed that all values of
206 the potential scale reduction factor (\hat{r}) converged to approximately 1.0 (Gelman et al. 2015). A
207 well-known issue with MCMC sampling using horseshoe priors when dealing with highly
208 correlated inputs (such as hyperspectral bands) and a low number of observations is that the \hat{r}
209 values of some individual regression coefficients do not converge to 1. However, this has been
210 shown not to cause any loss in the model’s predictive accuracy (Pironen and Vehtari 2017a). A
211 distinct advantage of Bayesian paradigm is that it provides us with a formal way to assess how the
212 model performs via posterior predictive checks. We use posterior predictive checks (Gabry et al.
213 2019) to simulate the posterior predictive distribution $p(\hat{y}|\mathbf{y}) = \int p(\hat{y}|\boldsymbol{\theta})p(\boldsymbol{\theta}|\mathbf{y})d\boldsymbol{\theta}$, where \mathbf{y} is the
214 training trait data, \hat{y} is the predicted data and $\boldsymbol{\theta}$ are the parameters of the model. Posterior
215 predictive checks serve as an important visual tool to assess how well the model agrees with the
216 training data.

217 **3.2.2 Model reduction in original spectral space**

218 The full Bayesian model in Section 3.2.1 makes use of all the input wavelengths to predict new
219 data, and thus has a high computational cost as well needs to store the posterior samples for all
220 2001 wavelengths. We remedy this by defining a model which takes a relevant subset of the input
221 hyperspectral wavelengths (of length l_s) as input while still mimicking the predictive capability of
222 the full model. Therefore, our aim is to find a sub-model:

$$\begin{aligned}
y_i &= \mu_s(x_{s,i}) + \epsilon_{s,i} \\
&= \beta_s^T \mathbf{x}_{s,i} + \epsilon_{s,i}, \quad \epsilon_s \sim N(0, \sigma_s^2), \quad i = 1, \dots, n; \\
\mathbf{y} &= (y_1, \dots, y_n) = N_n(X_s \beta_s, \sigma_s^2 I)
\end{aligned} \tag{5}$$

223 which has similar predictive accuracy as the full Bayesian model in Section 3.2.1 but with $l_s \ll l$.
224 Note that this approach does not to find all wavelengths that are statistically related to the trait, but
225 instead finds a reduced model consisting of a minimal subset of wavelengths that has similar
226 predictive capability as the full model such that adding more wavelengths will not significantly
227 improve predictive accuracy (Piironen, Paasiniemi, and Vehtari 2020).

228 3.2.2.1 Projection of full model to reduced model

229 To formulate the reduced model, we use predictive projection inference (Piironen, Paasiniemi, and
230 Vehtari 2020), which consists of replacing the posterior distribution of the parameters of the full
231 model with the posterior distribution of the reduced model. Since our aim is to transfer the
232 predictive capabilities of the full model to a reduced one, the posterior projection is defined in
233 terms of the loss in posterior predictive accuracy of the trait y —in terms of the Kullback-Liebler
234 (KL) divergence (Kullback and Leibler 1951)—when the reduced model is used in place of the
235 full model. For posterior samples $\{\beta^m, (\sigma^2)^m\}_{m=1}^M$ from the full Bayesian model (Section 3.2.1),
236 and a candidate reduced model of size s with input wavelength matrix X_s (Equation 5) it can be
237 shown that this loss is minimized when the parameters of the reduced candidate model has the
238 following form:

$$\begin{aligned}
\beta_s^m &= (X_s^T X_s)^{-1} X_s^T \mu^m(X) = (X_s^T X_s)^{-1} X_s^T (X \beta^m) \\
(\sigma_s^2)^m &= (\sigma^2)^m + \frac{1}{n} \|X_s \beta_s^m - X \beta^m\|^2; \quad m = \{1, \dots, M\}
\end{aligned} \tag{6}$$

239 where $\|a - b\|^2$ —also called the L2 norm—computes the sum of the squared differences between
240 corresponding elements of the two vectors a and b . The solution for β_s is the least squares solution
241 for linear regression models with the trait observations \mathbf{y} replaced by the posterior samples of the
242 expected predictions $\{\mu^m(X) = X \beta^m\}_{m=1}^M$ of the full Bayesian model. The projected variance of

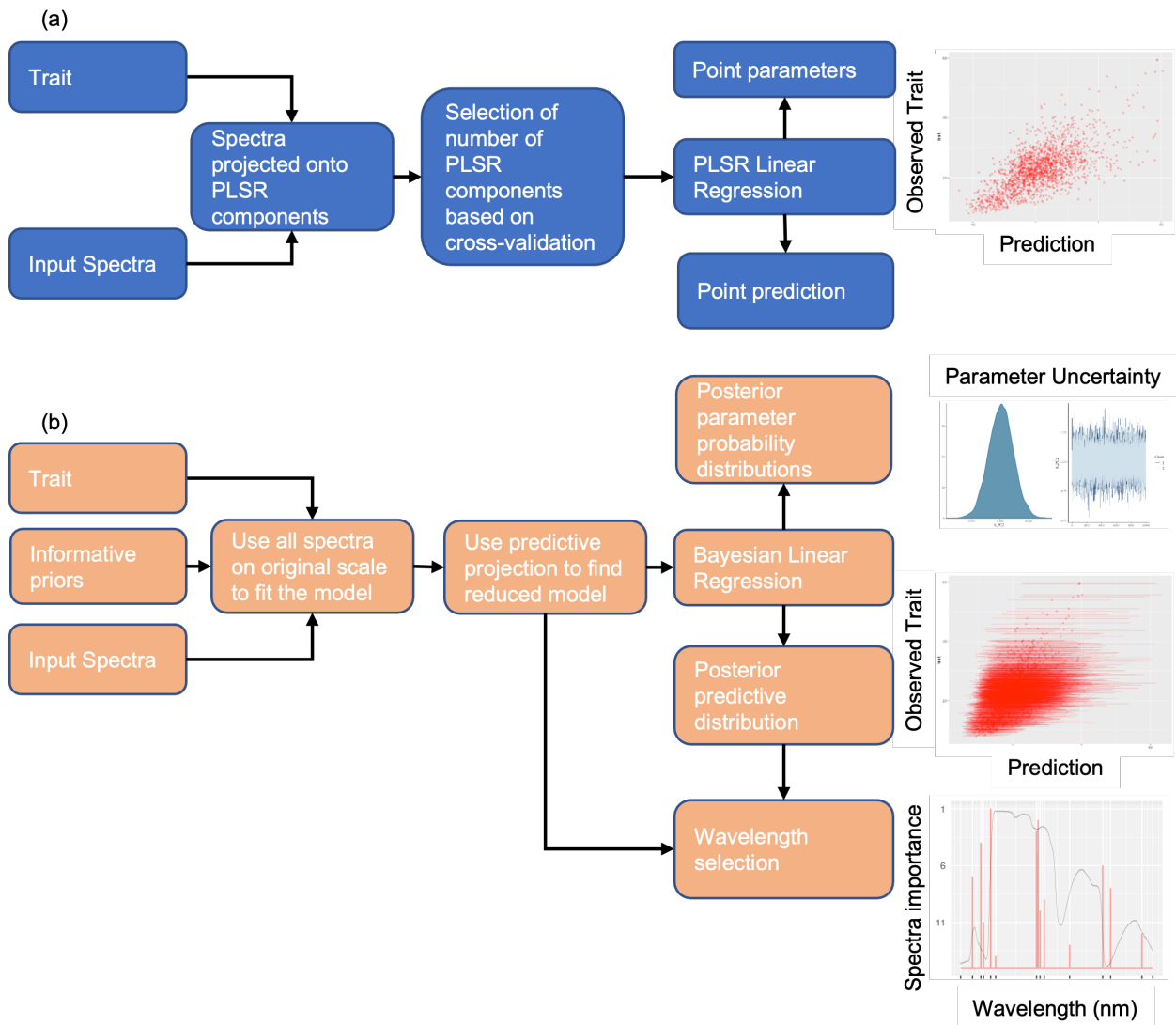


Figure 3: Comparison between (a) PLSR and (b) Bayesian approach. The Bayesian approach enables rigorous uncertainty quantification and uses all spectra on the original scale to fit the “full” regression model. To enhance computational efficiency and interpretation, the full model is projected onto the reduced model with similar predictive distribution.

243 the reduced model $(\sigma_s^2)^m$ denotes that it is equal to the variance of the full model plus systematic
244 variation captured by the full model but not by the reduced model. Hence, the predictive
245 uncertainty of the reduced model is always greater than or equal to the full model which helps
246 prevent over fitting of the reduced model (Piironen, Paasiniemi, and Vehtari 2020) and gives a
247 better measure of uncertainty when we trade off model complexity between the full and reduced
248 models. To get to the final reduced model, we have two considerations: (1) selecting wavelength
249 bands for the model of size s , since a large number of candidate models exist for a given model
250 size s , and (2) selecting the size of the final reduced model s_{final} . Since this leads to a huge
251 number of candidate models, we adopt the search heuristic which, starting from an intercept-only
252 reduced model, adds one wavelength at a time (using forward variable selection) minimizing the
253 KL-divergence among all the possible wavelengths up to a predetermined maximum number of
254 wavelengths (40 wavelengths in our study). The final size of the model $s_{final} \leq 40$ is chosen which
255 minimizes the k-cross validation root mean squared error (RMSE) between the full and reduced
256 model. Further details of the implementation can be found in (Piironen, Paasiniemi, and Vehtari
257 2020). The projection is done with the help of R package `projpred` (Piironen et al. 2023).
258 We also compared our new algorithm results against established best practices (e.g., Serbin et al.
259 2012) for estimating traits using PLSR. Similar to the Bayesian approach, we standardized the
260 input wavelengths to have a mean 0 and standard deviation 1 and used minimization of PRESS
261 (Allen 1971) in cross validation to determine the number of orthogonal PLSR components.

262 **4 Results**

263 **4.1 Full Bayesian model**

264 **4.1.1 Validation of the algorithms**

265 For all three traits, we use the posterior predictive checks (Figure 4) to see how well the fitted
266 Bayesian models simulate the training data which help us to determine the fit of the model to
267 training observations. The colored lines represent 1000 replications of the training data simulated

268 from the Bayesian models while the dark black line represents the empirical distribution of the
269 observations. In general, the overall fit for the three traits is satisfactory; potential improvements
270 to the Bayesian model are discussed in Section 5.3.

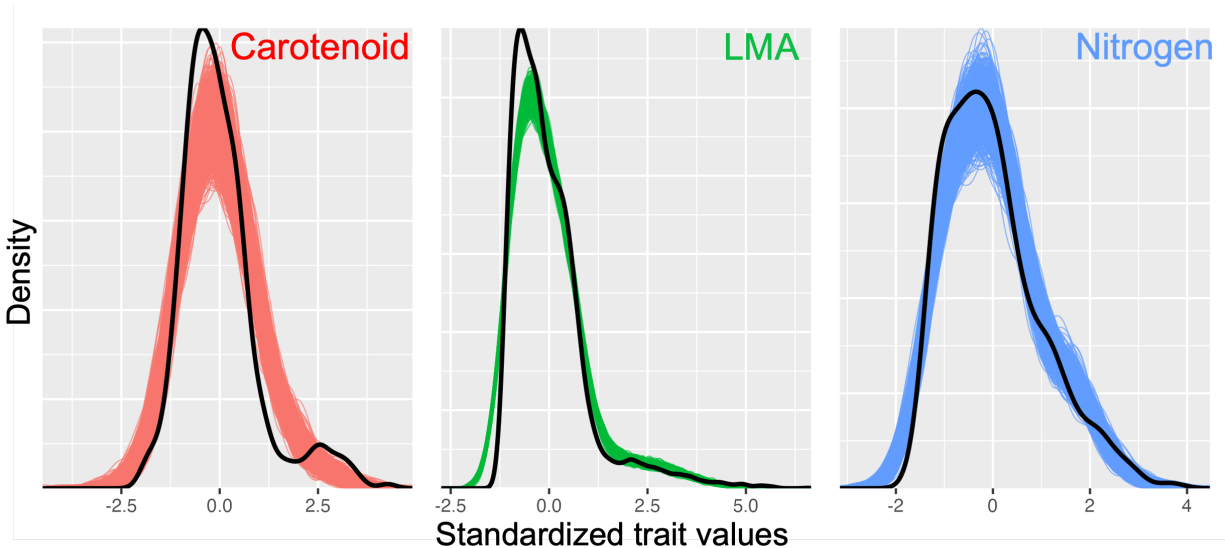


Figure 4: Posterior predictive checks for assessing model fit for the three traits depict how well the Bayesian models simulate the training data. The colored lines represents replications of the training data simulated with the Bayesian models, while the dark black line represents the empirical distribution of the observations.

271 For the validation (CABO) dataset, all three models did a satisfactory (but imperfect) job of
272 predicting all three traits. In terms of the root mean squared error (RMSE), we find that our full
273 model slightly outperformed PLSR for Car_A and LMA, and significantly outperformed PLSR for
274 N_M (Figure 5 and Table 1). For N_M , the large improvement in RMSE can be attributed to the
275 Bayesian approach correcting for an apparent bias in PLSR estimates. In terms of correlation (R),
276 our model performed very similarly to PLSR for Car_A and LMA but slightly worse than PLSR for
277 N_M .

278 For both Car_A and LMA data, both our Bayesian model and PLSR under-predicted high trait
279 values, especially for LMA and Car_A . This is similar to our findings from the posterior predictive
280 checks on training data, where Car_A and LMA have worse fits compared to N_M (Figure 4). The
281 Bayesian algorithm comes with the added advantage of providing posterior predictive uncertainty
282 along with the mean predictions, which allows us to assess the variability of our predictions

Table 1: Comparison of model performance (RMSE and R) for the validation dataset for Partial Least Squares Regression (PLSR), full Bayesian, and reduced Bayesian models. RMSE: Root mean squared error, R : Pearson correlation

Trait	Model	RMSE	R
Carotenoid ($\mu\text{g cm}^{-2}$)	PLSR	3.67	0.43
	Bayesian (Full)	3.62	0.43
	Bayesian (Reduced)	3.72	0.44
Nitrogen (mg g^{-1})	PLSR	7.17	0.64
	Bayesian (Full)	5.79	0.59
	Bayesian (Reduced)	5.62	0.61
Leaf Mass per Area (g m^{-2})	PLSR	31.79	0.84
	Bayesian (Full)	31.15	0.85
	Bayesian (Reduced)	30.96	0.84

283 associated with new datasets.

284 4.2 Reduced Bayesian model

285 We applied our projective inference technique (Section 3.2.2.1) to each of the three full Bayesian
 286 models. Using k-fold (5-fold for Car_A and N_M ; 3-fold for LMA) cross validation (Section 3.2.2.1),
 287 we find the minimal subset of wavelengths, such that adding more wavelengths to the model does
 288 not increase predictive accuracy when compared with the full Bayesian model. This results in 14
 289 wavelengths for Car_A , 28 for N_M , and 30 for LMA (Figure 6; Figure S1, SI). For some
 290 wavelengths, the regression coefficients exhibit much larger posterior intervals—such as at 1191
 291 nm and 1194 nm for Car_A (Figure 7)—often overlapping zero. This might lead to the incorrect
 292 assumption that these wavelengths are not important. However, this arises because, conditional on
 293 other variables in the model, the wavelengths are strongly correlated with each other. While this is
 294 not problematic for prediction, it means that with this model and data, we cannot isolate the
 295 marginal influence of the individual wavelengths on the trait (Car_A). We can only claim that a
 296 combination of these wavelengths influences the trait (McElreath 2018). In such cases, the
 297 posterior distributions of the regression coefficients align along a narrow ridge (Figure S2; SI),
 298 implying that, for each of the posterior samples, when the regression coefficient of one wavelength
 299 is large, the other is small. Consequently, a wide range of possible combinations of the two (or

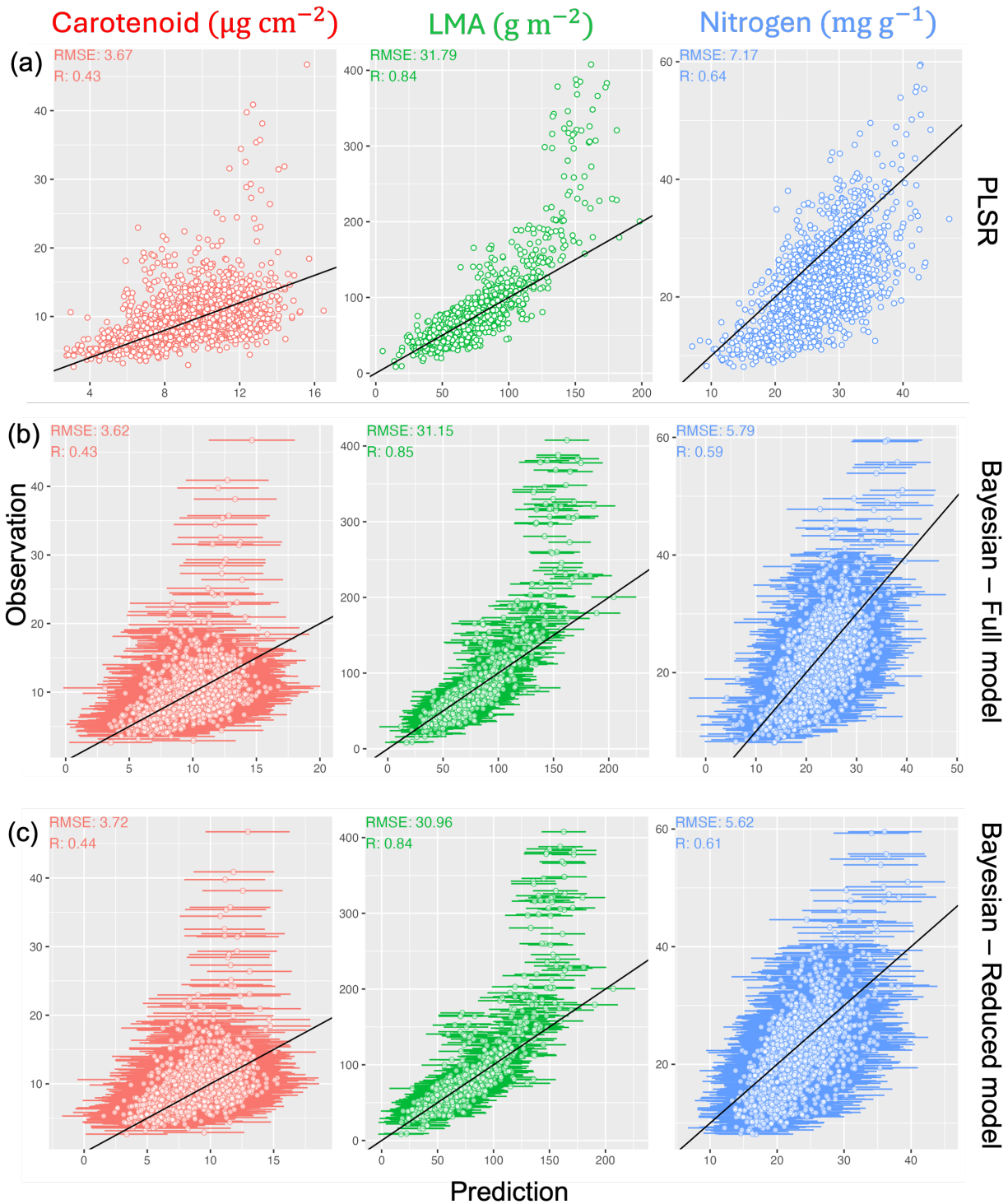


Figure 5: Comparison of (a) PLSR vs (b) full Bayesian vs (c) reduced Bayesian models on CABO test data. The Bayesian models perform similarly or slightly outperform the PLSR approach and provide rigorous uncertainty estimation. The horizontal bars for the Bayesian methods represent the 10th and 90th quantile posterior predictive intervals.

300 more) regression coefficients results in long univariate posterior parameter intervals. For
301 comparison, the PLSR regression coefficients for the traits are shown in Figure S3, SI.
302 For all three traits, the reduced Bayesian model performed comparably well to the full Bayesian
303 model (Figure 5 and Table 1). We find that the RMSE and R between the posterior mean of the
304 reduced model and the observations ($RMSE_{reduced}$ and $R_{reduced}$, respectively) are comparable to
305 those of the full model predictions for all three traits but at a fraction of the computational cost.
306 For predicting a large number of data, the posterior predictive technique can help speed up
307 computation time. For instance, on a 32 GB 2022 Macbook Pro, we resampled (with replacement)
308 the CABO data for each trait 50,000 times and computed the time to find posterior predictive
309 distribution using both the full (t_{full}) and reduced model ($t_{reduced}$) using 5000 posterior
310 parameter samples. Using the R package `microbenchmark` (Mersmann et al. 2023), we found a
311 considerable difference in the mean computational time for all three traits: Car_A ($t_{full} = 226$
312 seconds, $t_{reduced} = 68$ seconds) N_M ($t_{full} = 225$ seconds, $t_{reduced} = 104$ seconds) and LMA ($t_{full} =$
313 232 seconds, $t_{reduced} = 110$ seconds). The reduced model also allows us to store posterior
314 parameter samples for a select subset of the wavelengths as opposed to all wavelengths for the full
315 model.

316 **4.2.1 Important spectral regions for traits**

317 The reduced model finds a minimal subset of wavelengths (which are not necessarily unique) such
318 that adding more wavelengths to the model will not lead to a significant increase in the predictive
319 accuracy when compared with the full model. We can, however, still use the spectral ranks
320 (Figure 6), to identify the VSWIR regions that are important for predicting a particular trait.
321 For Car_A , the most important wavelength is in the red-edge region—characterized by a sudden
322 increase in leaf reflectance usually between 700 nm to 750 nm (Cotrozzi et al. 2018)—with
323 additional important wavelengths in the visible spectrum. Additionally, we find a cluster of
324 sensitive wavelength in the near infrared region (NIR) from 1150–1300 nm around a known
325 secondary water-absorption band at 1240 nm (Ustin and Jacquemoud 2020) and some
326 wavelengths in the short wave infrared region (SWIR) region (1300–2500 nm). For N_M , the

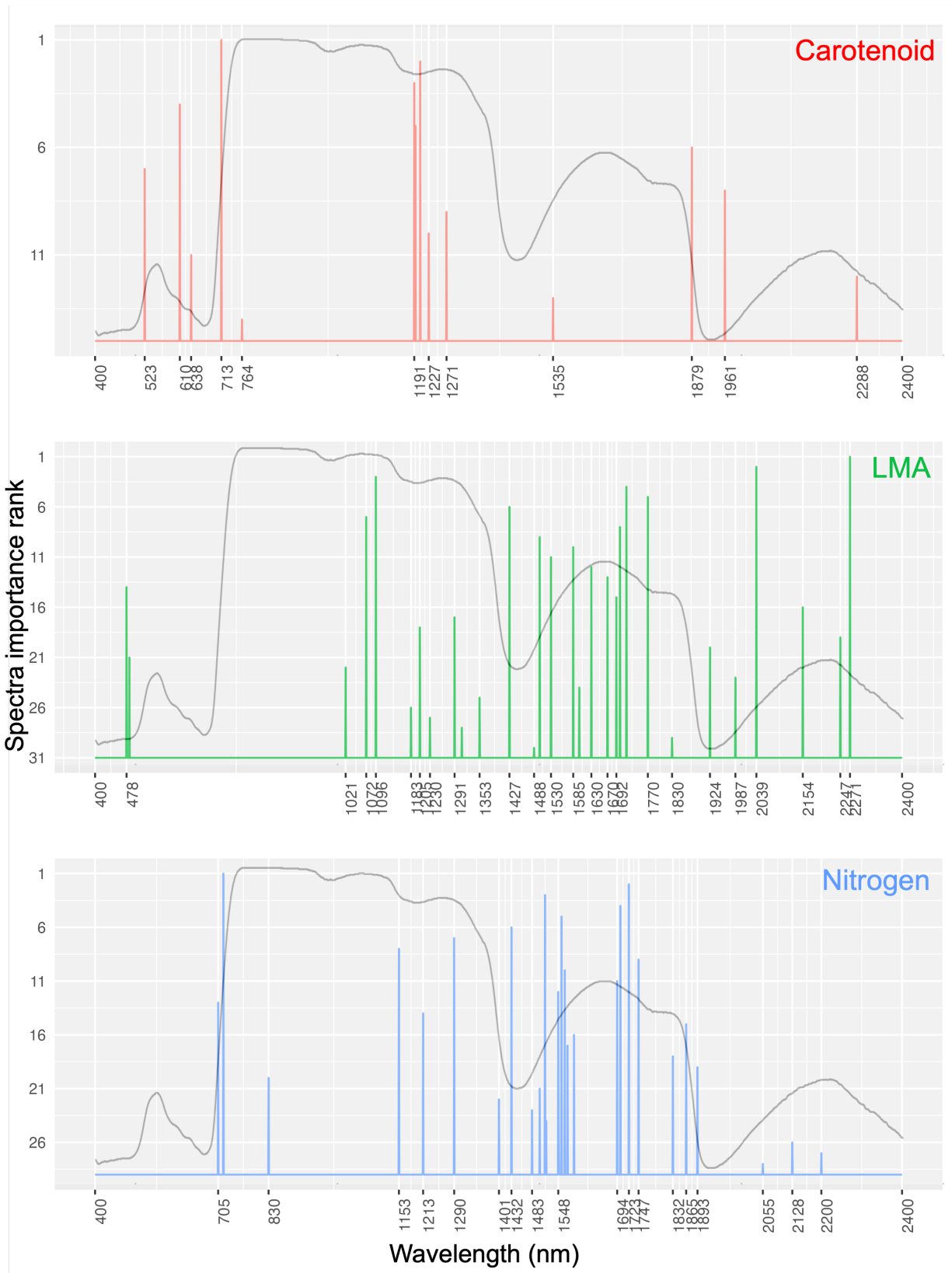


Figure 6: Relevant wavelengths for each trait using predictive projection. The spectral ranks denote the order in which the wavelengths are selected to minimize the difference in predictive accuracy between the full and reduced models at each step.



Figure 7: Posterior distribution for the projected parameters of the reduced model. Wavelengths that are correlated to each other have wider posterior intervals, due to a wide range of possible values for any posterior sample. This implies that we cannot distinguish the individual effects of such wavelengths on the trait.

327 red-edge again contains the most important wavelength with the rest of the important wavelengths
328 clustered in the SWIR region around 1400–1900 nm and 2000–2500 nm. The water absorption
329 band at 1240 nm also has some moderately important wavelengths clustered around it. For LMA,
330 wavelengths in the SWIR region are generally the most important: The two most important
331 wavelengths fall in the 2000–2500 nm region, while a cluster of important wavelengths fall in the
332 1500–2000 nm region. The variable influence on projection (VIP) metric plots (Mehmood et al.
333 2012) for the PLSR models, used to identify spectral regions that contribute significantly to trait
334 prediction, are shown in Figure S4, SI. While the VIP plots highlight important spectral regions,
335 they do not readily facilitate explicit wavelength selection.

336 **5 Discussion**

337 **5.1 Comparison of the algorithms**

338 In terms of accuracy, the proposed Bayesian algorithm works comparably to the PLSR algorithm
339 while also providing some important advantages. First, the Bayesian method works in the original
340 spectral space as opposed to a transformed latent scale, which makes the regression coefficients
341 conceptually simpler to understand and allows more flexibility to apply the algorithms to different
342 instruments with different spectral configurations. Since there is no spectral transformation, it
343 paves the way for future work incorporating input spectral uncertainty in trait estimation. Input
344 spectral uncertainty becomes especially important when statistical algorithms are applied to
345 remote sensing data, such as airborne and satellite data, which are subject to errors due to the
346 effects of various atmospheric and topographical factors on remote sensing retrievals (Thompson
347 et al. 2018).

348 Additionally, although PLSR methods can also account for predictive uncertainties using
349 resampling techniques such as bootstrapping (Singh et al. 2015), this uncertainty attempts to
350 approximate a non-informative posterior distribution by generally assuming that the training
351 sample closely approximates the true population which has been shown to produce inaccurate
352 confidence intervals for small to moderate sample sizes (Chernick and Labudde 2009; Hesterberg

2015). The Bayesian method provides rigorous uncertainty quantification in the form of posterior predictive credible intervals, which are easier to interpret than frequentist confidence intervals. Furthermore, our Bayesian method provides not only estimates of univariate (band-specific) uncertainties but also an estimate of the full joint posterior uncertainties (variance-covariance matrix) in regression coefficients (e.g., Figure S2, SI) across all input bands, helping us understand how information with respect to a trait is shared across bands. Finally, the Bayesian paradigm allows for natural incorporation of prior information which has been shown to improve retrievals of biophysical variables from reflectance (Combal et al. 2003).

5.2 Important spectral regions for traits

Carotenoids provide crucial information about plant status that is closely related to chlorophyll content. The balance between these two pigments serves as a phenological indicator, relying on distinctive absorbance and reflectance features in the green-red (500–690 nm) and red edge (700–800 nm) spectral ranges (Penuelas, Baret, and Filella 1995). The proposed Bayesian model identified five relevant bands around 520 nm, 610 nm, 640 nm, 710 nm, and 760 nm. These bands and regions have been suggested in previous research for estimating carotenoid content in leaves (Gitelson et al. 2002; Ustin and Jacquemoud 2020; Falcioni et al. 2023). We also found important wavelengths in the NIR and SWIR regions close to spectral features related to water absorption, leaf structure, and dry matter content (Ustin and Jacquemoud 2020; Serbin et al. 2019). Car_A has been shown to change with leaf growth stage and is affected by water stress (Mibei et al. 2016), potentially explaining the sensitivity of the above wavelengths to Car_A .

We found that the red-edge region was also important for predicting N_M . N_M has been shown to be correlated with chlorophyll content (Homolová et al. 2013), which has strong absorption in the red region and therefore strongly influences the magnitude and position of the red-edge. We also found a cluster of important wavelengths around the water absorption region at 1200 nm that have also been shown to be sensitive to N_M in past research (Homolová et al. 2013). Our findings also show multiple bands in the SWIR region were critical to predicting N_M , likely because proteins have distinct absorption features in this region (Fourty et al. 1996; Curran 1989; Kumar et al.

2001) and a large amount of leaf nitrogen is bound in proteins (Xu et al. 2012). This has led to a recent push in recognizing proteins (in addition to chlorophyll) as a proxy for estimating leaf nitrogen (Berger et al. 2020).

Our findings show that the SWIR region was the most important for predicting LMA, especially wavelengths in the 1500–1800 nm and 2000–2300 nm regions. This corresponds to the wavelengths reported by Cheng et al. (2014) deriving LMA from foliar reflectance across several species using observations and radiative transfer models. LMA has also been shown to be correlated with different leaf features related to structure, dry matter, carbon, and leaf water content, which have absorption features in the SWIR region (Poorter et al. 2009; Riva et al. 2016; Curran 1989; Kokaly et al. 2009; Ustin and Jacquemoud 2020; Serbin et al. 2019). The NIR region between 1000–1300 nm is also seen to be useful in predicting LMA, which is consistent with the findings of Serbin et al. (2019), who posited that this dependence is driven by the covariation of LMA with other molecules and related leaf attributes with strong NIR absorption features—leaf water, structural carbon, leaf thickness, and variations in the epidermis layer of the leaf.

5.3 Limitations and future directions

In this work, we have restricted ourselves to using a linear Gaussian model with a fixed measurement error. However, a simple linear model might not be sufficient to characterize the effects of spectra on traits (Figure 4). A distinct advantage of Bayesian methods is their ability to easily add complexity to an existing model structure. There are various ways in which we can extend the current Bayesian model. First, we can relax the assumption of a Gaussian model for the traits and experiment with other probability density functions, such as Gamma distributions, Student-t distributions, and mixture models. In this work, we have restricted ourselves to using a linear Gaussian model with a fixed measurement error. However, a simple linear model might not be sufficient to characterize the effects of spectra on traits (Figure 4). A distinct advantage of Bayesian methods is their ability to easily add complexity to an existing model structure. There are various ways in which we can extend the current Bayesian model. First, we can relax the

407 assumption of a Gaussian model for the traits and experiment with other probability density
408 functions, such as Gamma distributions, Student-t distributions, and mixture models. This work
409 assumes homoscedastic measurement error, such that the error variance (σ^2) remains constant
410 across all observations (Figure S5, SI). This assumption could be relaxed by allowing the
411 measurement error to be heteroscedastic, enabling the variance to vary with the trait values. We
412 will extend this work to more traits, such as chlorophyll, leaf water content, cellulose, lignin,
413 calcium, phosphorous, magnesium, etc., using appropriate density functions and measurement
414 errors. Second, we can extend the model to a hierarchical setup by recognizing the inherent
415 groups that exist in plants, such as broadleaf vs. needleleaf or deciduous vs. evergreen. Bayesian
416 hierarchical methods explicitly accommodate variability in the relationship between traits and
417 spectra across different groups, effectively sharing information and improving parameter
418 estimation (which is especially important for undersampled groups). Such analysis will help in
419 improving the model-transferability of the Bayesian models across different regions, seasons, and
420 plant functional types — a known limitation of PLSR-based approaches as well as the current
421 linear Bayesian setup presented here, which does not explicitly account for variability across plant
422 functional types or biomes. Doing this analysis however requires datasets with sufficient coverage
423 and balance across plant functional types, biomes, and environmental gradients (Jia et al. 2024),
424 as well as careful consideration of how the hierarchy is constructed — for instance, whether to
425 group by plant functional type, biome, or phylogeny — and how to meaningfully incorporate
426 scientific prior knowledge into the hierarchical structure. We therefore identify this as an
427 important and non-trivial direction for future work, and defer a full treatment to a subsequent
428 study. The linear relationship between spectra and traits is another assumption that can be
429 challenged, and Bayesian methods are easily amenable to including non-linear effects of spectra
430 on traits (Gelman et al. 2015).

431 Another opportunity for Bayesian methods is in multivariate prediction, wherein we explicitly
432 account for the covariance between multiple predicted traits (Shiklomanov, Cowdery, et al. 2020).
433 This can be done by assuming a multivariate normal distribution of traits (with a covariance
434 matrix denoting how the traits covary with each other). Another approach that can be utilized is

435 using Directed Acyclic Graphs (DAGs) (McElreath 2018), which can also be used to disentangle
436 the latent relationships existing between different trait values (e.g., Chadwick and Asner 2016)
437 and to distinguish between the so-called optically “visible” traits (traits that correspond to specific
438 molecules known to influence leaf optical properties, such as pigments, water, and structural
439 molecules) and the “invisible” traits (traits that have minimal or no direct influence on leaf optical
440 properties but which can be estimated because of their covariance with visible traits; examples
441 include micronutrients, isotopic ratios, and rates of photosynthesis or respiration). A causal
442 approach such as DAGs can also help disentangle the effects of spectra on “composite” traits (such
443 as nitrogen, which is found in both proteins and pigments) into sub-component spectra-trait
444 relationships. Such an approach can also inform physically based model improvement.
445 We restricted ourselves to leaf-level prediction of traits, but the Bayesian algorithm—and its
446 extensions—are equally applicable to remote sensing imaging spectroscopy. It is an exciting time
447 for hyperspectral imaging spectroscopy with the recently launched and upcoming satellite
448 missions, such as PRecursores IperSpettrale della Missione Applicativa (PRISMA, Cogliati et al.
449 2021), Earth Surface Mineral Dust Source Investigation (EMIT, Green 2022), Environmental
450 Mapping and Analysis Program (EnMAP, Guanter et al. 2015), Surface Biology and Geology
451 (SBG, Cawse-Nicholson et al. 2021), and Copernicus Hyperspectral Imaging Mission for the
452 Environment (CHIME, Nieke et al. 2023), which are poised to provide vast troves of VSWIR data
453 globally. The uncertainty quantification arising due to different sensor characteristics,
454 spatio-temporal sampling scales, and sub-pixel heterogeneity makes it all the more important to
455 perform rigorous uncertainty quantification, and therefore, the use of Bayesian methods becomes
456 even more crucial in such scenarios. Furthermore, Bayesian methods are well-suited to rigorously
457 propagate uncertainties from the input reflectance, such as those introduced by Bayesian
458 atmospheric correction algorithms (e.g., ISOFIT Thompson et al. 2018), as well as variability
459 arising from solar and viewing geometry (Schaeppman-Strub et al. 2006; Queally et al. 2022), to
460 the estimated traits.

461 **6 Conclusion**

462 In this paper, we present a computationally efficient Bayesian framework that estimates traits
463 directly from reflectance spectra without latent transformation while rigorously propagating
464 uncertainties. The results show that the Bayesian model performs comparably to the PLSR
465 approach for the three traits examined, while providing the advantages of working in the original
466 spectral space, selecting relevant wavelengths for predictions, and offering posterior predictive
467 uncertainties, which aid in assessing the variability of predictions on new datasets. The Bayesian
468 framework is extendable to more complex models—such as non-linear models, hierarchical
469 Bayesian models and multivariate trait prediction models— can integrate with physical models and
470 account for measurement errors of different instruments.

471 **7 Acknowledgements**

472 We acknowledge the helpful comments of Frank Weber and Aki Vehtari. This work was
473 supported by the NASA ROSES New (Early Career) Investigator Program in Earth Science
474 (NNH20ZDA001N-NIP; proposal number 20-NIP20-0134) and the NASA ROSES Earth Surface
475 Mineral Dust Source Investigation (EMIT) Science and Applications Team
476 (NNH23ZDA001N-EMIT; proposal number 23-EMIT23-0039).

477 **8 Author Contributions**

478 Kathuria and Shiklomanov conceived the ideas and designed methodology; Kathuria compiled the
479 data; Kathuria and Lang analysed the data; Kathuria led the writing of the manuscript.
480 Shiklomanov and Angel edited and gave critical inputs for the manuscript draft, and all authors
481 gave final approval for publication.

9 Conflict of Interest Statement

The authors have no conflict of interest to declare.

References

Allen, David M. 1971. “Mean Square Error of Prediction as a Criterion for Selecting Variables.” *Technometrics* 13 (3): 469–75. <https://doi.org/10.2307/1267161>.

Angel, Yoseline, and Alexey N. Shiklomanov. 2022. “Remote Detection and Monitoring of Plant Traits: Theory and Practice.” In, edited by Jeremy A Roberts, 1st ed., 313–44. Wiley. <https://doi.org/10.1002/9781119312994.apr0778>.

Armstrong, G. A., and J. E. Hearst. 1996. “Carotenoids 2: Genetics and molecular biology of carotenoid pigment biosynthesis.” *FASEB journal: official publication of the Federation of American Societies for Experimental Biology* 10 (2): 228–37. <https://doi.org/10.1096/fasebj.10.2.8641556>.

Berger, Katja, Jochem Verrelst, Jean-Baptiste Féret, Zhihui Wang, Matthias Woche, Markus Strathmann, Martin Danner, Wolfram Mauser, and Tobias Hank. 2020. “Crop Nitrogen Monitoring: Recent Progress and Principal Developments in the Context of Imaging Spectroscopy Missions.” *Remote Sensing of Environment* 242 (June): 111758. <https://doi.org/10.1016/j.rse.2020.111758>.

Betancourt, Michael. 2017. “A Conceptual Introduction to Hamiltonian Monte Carlo.” <https://arxiv.org/abs/1701.02434v2>.

Bürkner, Paul-Christian. 2017. “Brms: An R Package for Bayesian Multilevel Models Using Stan.” *Journal of Statistical Software* 80 (August): 1–28. <https://doi.org/10.18637/jss.v080.i01>.

Burnett, Angela C, Jeremiah Anderson, Kenneth J Davidson, Kim S Ely, Julien Lamour, Qianyu Li, Bailey D Morrison, Dedi Yang, Alistair Rogers, and Shawn P Serbin. 2021. “A Best-Practice Guide to Predicting Plant Traits from Leaf-Level Hyperspectral Data Using

507 Partial Least Squares Regression.” *Journal of Experimental Botany* 72 (18): 6175–89.
508 <https://doi.org/10.1093/jxb/erab295>.

509 Carvalho, Carlos M., Nicholas G. Polson, and James G. Scott. 2010. “The Horseshoe Estimator
510 for Sparse Signals.” *Biometrika* 97 (2): 465–80.
511 <https://www.jstor.org/stable/25734098>.

512 Cawse-Nicholson, Kerry, Philip A. Townsend, David Schimel, Ali M. Assiri, Pamela L. Blake,
513 Maria Fabrizia Buongiorno, Petya Campbell, et al. 2021. “NASA’s Surface Biology and
514 Geology Designated Observable: A Perspective on Surface Imaging Algorithms.” *Remote
515 Sensing of Environment* 257 (May): 112349.
516 <https://doi.org/10.1016/j.rse.2021.112349>.

517 Chadwick, K. Dana, and Gregory P. Asner. 2016. “Organismic-Scale Remote Sensing of Canopy
518 Foliar Traits in Lowland Tropical Forests.” *Remote Sensing* 8 (2): 87.
519 <https://doi.org/10.3390/rs8020087>.

520 Cheng, Tao, Benoit Rivard, Arturo G. Sánchez-Azofeifa, Jean-Baptiste Féret, Stéphane
521 Jacquemoud, and Susan L. Ustin. 2014. “Deriving Leaf Mass Per Area (LMA) from Foliar
522 Reflectance Across a Variety of Plant Species Using Continuous Wavelet Analysis.” *ISPRS
523 Journal of Photogrammetry and Remote Sensing* 87 (January): 28–38.
524 <https://doi.org/10.1016/j.isprsjprs.2013.10.009>.

525 Cherif, Eya, Hannes Feilhauer, Katja Berger, Phuong D. Dao, Michael Ewald, Tobias B. Hank,
526 Yuhong He, et al. 2023. “From Spectra to Plant Functional Traits: Transferable Multi-Trait
527 Models from Heterogeneous and Sparse Data.” *Remote Sensing of Environment* 292 (July):
528 113580. <https://doi.org/10.1016/j.rse.2023.113580>.

529 Chernick, Michael R., and Robert A. Labudde. 2009. “Revisiting Qualms about Bootstrap
530 Confidence Intervals.” *American Journal of Mathematical and Management Sciences* 29
531 (3-4): 437–56. <https://doi.org/10.1080/01966324.2009.10737767>.

532 Cogliati, S., F. Sarti, L. Chiarantini, M. Cosi, R. Lorusso, E. Lopinto, F. Miglietta, et al. 2021.
533 “The PRISMA Imaging Spectroscopy Mission: Overview and First Performance Analysis.”
534 *Remote Sensing of Environment* 262 (September): 112499.

535 <https://doi.org/10.1016/j.rse.2021.112499>.

536 Combal, B, F Baret, M Weiss, A Trubuil, D Macé, A Pragnère, R Myneni, Y Knyazikhin, and L
537 Wang. 2003. “Retrieval of Canopy Biophysical Variables from Bidirectional Reflectance:
538 Using Prior Information to Solve the Ill-Posed Inverse Problem.” *Remote Sensing of*
539 *Environment* 84 (1): 1–15. [https://doi.org/10.1016/S0034-4257\(02\)00035-4](https://doi.org/10.1016/S0034-4257(02)00035-4).

540 Cornelissen, J. H. C., and K. Thompson. 1997. “Functional Leaf Attributes Predict Litter
541 Decomposition Rate in Herbaceous Plants.” *New Phytologist* 135 (1): 109–14.
542 <https://doi.org/10.1046/j.1469-8137.1997.00628.x>.

543 Cotrozzi, Lorenzo, Philip A. Townsend, Elisa Pellegrini, Cristina Nali, and John J. Couture. 2018.
544 “Reflectance Spectroscopy: A Novel Approach to Better Understand and Monitor the Impact
545 of Air Pollution on Mediterranean Plants.” *Environmental Science and Pollution Research* 25
546 (9): 8249–67. <https://doi.org/10.1007/s11356-017-9568-2>.

547 Curran, Paul J. 1989. “Remote Sensing of Foliar Chemistry.” *Remote Sensing of Environment* 30
548 (3): 271–78. [https://doi.org/10.1016/0034-4257\(89\)90069-2](https://doi.org/10.1016/0034-4257(89)90069-2).

549 Datta, Jyotishka, and Jayanta K. Ghosh. 2013. “Asymptotic Properties of Bayes Risk for the
550 Horseshoe Prior.” *Bayesian Analysis* 8 (1): 111–32.
551 <https://doi.org/10.1214/13-BA805>.

552 Duane, Simon, Anthony D. Kennedy, Brian J. Pendleton, and Duncan Roweth. 1987. “Hybrid
553 Monte Carlo.” *Physics Letters B* 195 (2): 216–22.

554 Erp, Sara van, Daniel L. Oberski, and Joris Mulder. 2019. “Shrinkage Priors for Bayesian
555 Penalized Regression.” *Journal of Mathematical Psychology* 89 (April): 31–50.
556 <https://doi.org/10.1016/j.jmp.2018.12.004>.

557 Evans, John R, and Victoria C Clarke. 2019. “The Nitrogen Cost of Photosynthesis.” *Journal of*
558 *Experimental Botany* 70 (1): 7–15. <https://doi.org/10.1093/jxb/ery366>.

559 Falcioni, Renan, Werner Camargos Antunes, José Alexandre Melo Demattê, and Marcos Rafael
560 Nanni. 2023. “A Novel Method for Estimating Chlorophyll and Carotenoid Concentrations in
561 Leaves: A Two Hyperspectral Sensor Approach.” *Sensors (Basel, Switzerland)* 23 (8): 3843.
562 <https://doi.org/10.3390/s23083843>.

563 Fourty, Th., F. Baret, S. Jacquemoud, G. Schmuck, and J. Verdebout. 1996. “Leaf Optical
564 Properties with Explicit Description of Its Biochemical Composition: Direct and Inverse
565 Problems.” *Remote Sensing of Environment* 56 (2): 104–17.
566 [https://doi.org/10.1016/0034-4257\(95\)00234-0](https://doi.org/10.1016/0034-4257(95)00234-0).

567 Friedlingstein, P., P. Cox, R. Betts, L. Bopp, W. von Bloh, V. Brovkin, P. Cadule, et al. 2006.
568 “Climate–Carbon Cycle Feedback Analysis: Results from the C4MIP Model
569 Intercomparison.” *Journal of Climate* 19 (14): 3337–53.
570 <https://doi.org/10.1175/JCLI3800.1>.

571 Gabry, Jonah, Daniel Simpson, Aki Vehtari, Michael Betancourt, and Andrew Gelman. 2019.
572 “Visualization in Bayesian Workflow.” *Journal of the Royal Statistical Society Series A:*
573 *Statistics in Society* 182 (2): 389–402. <https://doi.org/10.1111/rssa.12378>.

574 Gelfand, Alan E., Li Zhu, and Bradley P. Carlin. 2001. “On the Change of Support Problem for
575 Spatio-Temporal Data.” *Biostatistics* 2 (1): 31–45.
576 <https://doi.org/10.1093/biostatistics/2.1.31>.

577 Gelman, Andrew, John B. Carlin, Hal S. Stern, David B. Dunson, Aki Vehtari, and Donald B.
578 Rubin. 2015. *Bayesian Data Analysis*. 3rd ed. New York: Chapman; Hall/CRC.
579 <https://doi.org/10.1201/b16018>.

580 Gitelson, Anatoly A., Yoav Zur, Olga B. Chivkunova, and Mark N. Merzlyak. 2002. “Assessing
581 Carotenoid Content in Plant Leaves with Reflectance Spectroscopy.” *Photochemistry and*
582 *Photobiology* 75 (3): 272–81.
583 [https://doi.org/10.1562/0031-8655\(2002\)0750272ACCIPL2.0.CO2](https://doi.org/10.1562/0031-8655(2002)0750272ACCIPL2.0.CO2).

584 Green, Robert O. 2022. “IGARSS 2022 - 2022 IEEE International Geoscience and Remote
585 Sensing Symposium.” In, 5004–6.
586 <https://doi.org/10.1109/IGARSS46834.2022.9883479>.

587 Guanter, Luis, Hermann Kaufmann, Karl Segl, Saskia Foerster, Christian Rogass, Sabine
588 Chabrillat, Theres Kuester, et al. 2015. “The EnMAP Spaceborne Imaging Spectroscopy
589 Mission for Earth Observation.” *Remote Sensing* 7 (7): 8830–57.
590 <https://doi.org/10.3390/rs70708830>.

- 591 Gustafson, Paul. 2003. *Measurement Error and Misclassification in Statistics and Epidemiology: Impacts and Bayesian Adjustments*. Chapman; Hall/CRC.
- 592
- 593 Hansen, P. M., and J. K. Schjoerring. 2003. “Reflectance Measurement of Canopy Biomass and Nitrogen Status in Wheat Crops Using Normalized Difference Vegetation Indices and Partial Least Squares Regression.” *Remote Sensing of Environment* 86 (4): 542–53.
- 594
- 595 [https://doi.org/10.1016/S0034-4257\(03\)00131-7](https://doi.org/10.1016/S0034-4257(03)00131-7).
- 596
- 597 Hesterberg, Tim C. 2015. “What Teachers Should Know about the Bootstrap: Resampling in the Undergraduate Statistics Curriculum.” *The American Statistician* 69 (4): 371–86.
- 598
- 599 <https://doi.org/10.1080/00031305.2015.1089789>.
- 600 Hoffman, Matthew D., and Andrew Gelman. 2014. “The No-u-Turn Sampler: Adaptively Setting Path Lengths in Hamiltonian Monte Carlo.” *J. Mach. Learn. Res.* 15 (1): 1593–623.
- 601
- 602 Homolová, Lucie, Zbyněk Malenovský, Jan G. P. W. Clevers, Glenda García-Santos, and Michael E. Schaepman. 2013. “Review of Optical-Based Remote Sensing for Plant Trait Mapping.” *Ecological Complexity* 15 (September): 1–16.
- 603
- 604 <https://doi.org/10.1016/j.ecocom.2013.06.003>.
- 605
- 606 Jacquemoud, Stéphane, and Susan Ustin. 2019. “Leaf Optical Properties.”
- 607 <https://www.cambridge.org/core/books/leaf-optical-properties/1E50A8985CB45AD9C70BAD3144D69E0C>.
- 608
- 609 Ji, F., F. Li, D. Hao, A. N. Shiklomanov, X. Yang, P. A. Townsend, H. Dashti, T. Nakaji, K. R. Kovach, H. Liu, M. Luo, and M. Chen. 2024. “Unveiling the transferability of PLSR models for leaf trait estimation: Lessons from a comprehensive analysis with a novel global dataset.” *New Phytologist* 243 (1): 111–131. <https://doi.org/10.1111/nph.19807>.
- 610
- 611
- 612
- 613 Kathuria, Dhruva, Binayak P. Mohanty, and Matthias Katzfuss. 2019. “Multiscale Data Fusion for Surface Soil Moisture Estimation: A Spatial Hierarchical Approach.” *Water Resources Research* 55 (12): 10443–65. <https://doi.org/10.1029/2018WR024581>.
- 614
- 615
- 616 Kokaly, Raymond F., Gregory P. Asner, Scott V. Ollinger, Mary E. Martin, and Carol A. Wessman. 2009. “Characterizing Canopy Biochemistry from Imaging Spectroscopy and Its Application to Ecosystem Studies.” *Remote Sensing of Environment*, Imaging spectroscopy special issue,
- 617
- 618

619 113 (September): S78–91. <https://doi.org/10.1016/j.rse.2008.10.018>.

620 Kothari, Shan, Rosalie Beauchamp-Rioux, Florence Blanchard, Anna L. Crofts, Alizée Girard,
621 Xavier Guilbeault-Mayers, Paul W. Hacker, et al. 2023. “Predicting Leaf Traits Across
622 Functional Groups Using Reflectance Spectroscopy.” *New Phytologist* 238 (2): 549–66.
623 <https://doi.org/10.1111/nph.18713>.

624 Kullback, S., and R. A. Leibler. 1951. “On Information and Sufficiency.” *The Annals of*
625 *Mathematical Statistics* 22 (1): 79–86. <https://doi.org/10.1214/aoms/1177729694>.

626 Kumar, Lalit, Karin Schmidt, Steve Dury, and Andrew Skidmore. 2001. “Imaging Spectrometry
627 and Vegetation Science.” In, edited by Freek D. van der Meer and Steven M. De Jong, 111–55.
628 Dordrecht: Springer Netherlands. https://doi.org/10.1007/978-0-306-47578-8_5.

629 Lavorel, S., and E. Garnier. 2002. “Predicting Changes in Community Composition and
630 Ecosystem Functioning from Plant Traits: Revisiting the Holy Grail.” *Functional Ecology* 16
631 (5): 545–56. <https://doi.org/10.1046/j.1365-2435.2002.00664.x>.

632 McElreath, Richard. 2018. *Statistical Rethinking: A Bayesian Course with Examples in r and*
633 *Stan*. Chapman; Hall/CRC.

634 Mehmood, T., K. H. Liland, L. Snipen, and S. Sæbø. 2012. “A review of variable selection
635 methods in partial least squares regression.” *Chemometrics and Intelligent Laboratory*
636 *Systems* 118: 62–69. <https://doi.org/10.1016/j.chemolab.2012.07.010>.

637 Mersmann, Olaf, Claudia Beleites, Rainer Hurling, Ari Friedman, and Joshua M. Ulrich. 2023.
638 *Microbenchmark: Accurate Timing Functions*.
639 <https://cran.r-project.org/web/packages/microbenchmark/>.

640 Mibei, Elias K., Jane Ambuko, James J. Giovannoni, Arnold N. Onyango, and Willis O. Owino.
641 2016. “Carotenoid Profiling of the Leaves of Selected African Eggplant Accessions Subjected
642 to Drought Stress.” *Food Science & Nutrition* 5 (1): 113–22.
643 <https://doi.org/10.1002/fsn3.370>.

644 Nieke, Jens, Laurent Despoisse, Antonio Gabriele, Heidrun Weber, Helene Strese, Nafiseh
645 Ghasemi, Ferran Gascon, et al. 2023. “Sensors, Systems, and Next-Generation Satellites
646 XXVII.” In, 12729:21–40. SPIE. <https://doi.org/10.1117/12.2679977>.

647 O'Hagan, Anthony, and Mike West, eds. 2013. *The Oxford Handbook of Applied Bayesian*
648 *Analysis*. Oxford University Press.
649 <https://doi.org/10.1093/oxfordhb/9780198703174.001.0001>.

650 Onoda, Yusuke, Ian J. Wright, John R. Evans, Kouki Hikosaka, Kaoru Kitajima, Ülo Niinemets,
651 Hendrik Poorter, Tiina Tosens, and Mark Westoby. 2017. "Physiological and Structural
652 Tradeoffs Underlying the Leaf Economics Spectrum." *New Phytologist* 214 (4): 1447–63.
653 <https://doi.org/10.1111/nph.14496>.

654 Oren, R., E. -D. Schulze, R. Matyssek, and R. Zimmermann. 1986. "Estimating Photosynthetic
655 Rate and Annual Carbon Gain in Conifers from Specific Leaf Weight and Leaf Biomass."
656 *Oecologia* 70 (2): 187–93. <https://doi.org/10.1007/BF00379238>.

657 Osnas, Jeanne L. D., Jeremy W. Lichstein, Peter B. Reich, and Stephen W. Pacala. 2013. "Global
658 Leaf Trait Relationships: Mass, Area, and the Leaf Economics Spectrum." *Science* 340
659 (6133): 741–44. <https://doi.org/10.1126/science.1231574>.

660 Penuelas, J, Frédéric Baret, and I Filella. 1995. "Semi-Empirical Indices to Assess
661 Carotenoids/Chlorophyll a Ratio from Leaf Spectral Reflectance." *Photosynthetica* 31 (2):
662 221–30.

663 Pereira, H. M., S. Ferrier, M. Walters, G. N. Geller, R. H. G. Jongman, R. J. Scholes, M. W.
664 Bruford, et al. 2013. "Essential Biodiversity Variables." *Science* 339 (6117): 277–78.
665 <https://doi.org/10.1126/science.1229931>.

666 Pettorelli, Nathalie, Martin Wegmann, Andrew Skidmore, Sander Múcher, Terence P. Dawson,
667 Miguel Fernandez, Richard Lucas, et al. 2016. "Framing the Concept of Satellite Remote
668 Sensing Essential Biodiversity Variables: Challenges and Future Directions." *Remote Sensing*
669 *in Ecology and Conservation* 2 (3): 122–31. <https://doi.org/10.1002/rse2.15>.

670 Piironen, Juho, Markus Paasiniemi, Alejandro Catalina, Frank Weber, and Aki Vehtari. 2023.
671 "projpred: Projection Predictive Feature Selection." <https://mc-stan.org/projpred/>.

672 Piironen, Juho, Markus Paasiniemi, and Aki Vehtari. 2020. "Projective Inference in
673 High-Dimensional Problems: Prediction and Feature Selection." *Electronic Journal of*
674 *Statistics* 14 (1): 2155–97. <https://doi.org/10.1214/20-EJS1711>.

675 Piironen, Juho, and Aki Vehtari. 2017a. “Sparsity Information and Regularization in the
676 Horseshoe and Other Shrinkage Priors.” *Electronic Journal of Statistics* 11 (2): 5018–51.
677 <https://doi.org/10.1214/17-EJS1337SI>.

678 ———. 2017b. “Comparison of Bayesian Predictive Methods for Model Selection.” *Statistics
679 and Computing* 27 (3): 711–35. <https://doi.org/10.1007/s11222-016-9649-y>.

680 Poorter, Hendrik, Ülo Niinemets, Lourens Poorter, Ian J. Wright, and Rafael Villar. 2009. “Causes
681 and Consequences of Variation in Leaf Mass Per Area (LMA): A Meta-Analysis.” *New
682 Phytologist* 182 (3): 565–88. <https://doi.org/10.1111/j.1469-8137.2009.02830.x>.

683 Pullanagari, R. R., Gábor Kereszturi, and I. J. Yule. 2016. “Mapping of Macro and Micro
684 Nutrients of Mixed Pastures Using Airborne AisaFENIX Hyperspectral Imagery.” *ISPRS
685 Journal of Photogrammetry and Remote Sensing* 117 (July): 1–10.
686 <https://doi.org/10.1016/j.isprsjprs.2016.03.010>.

687 Queally, N., Z. Ye, T. Zheng, A. Chlus, F. Schneider, R. P. Pavlick, and P. A. Townsend. 2022.
688 “FlexBRDF: A flexible BRDF correction for grouped processing of airborne imaging
689 spectroscopy flightlines.” *Journal of Geophysical Research: Biogeosciences* 127 (1):
690 e2021JG006622. <https://doi.org/10.1029/2021JG006622>.

691 Riva, Enrique G. de la, Manuel Olmo, Hendrik Poorter, José Luis Ubera, and Rafael Villar. 2016.
692 “Leaf Mass Per Area (LMA) and Its Relationship with Leaf Structure and Anatomy in 34
693 Mediterranean Woody Species Along a Water Availability Gradient.” *PLOS ONE* 11 (2):
694 e0148788. <https://doi.org/10.1371/journal.pone.0148788>.

695 Schaepman-Strub, G., M. E. Schaepman, T. H. Painter, S. Dangel, and J. V. Martonchik. 2006.
696 “Reflectance quantities in optical remote sensing—Definitions and case studies.” *Remote
697 Sensing of Environment* 103 (1): 27–42.
698 <https://doi.org/10.1016/j.rse.2006.03.002>.

699 Serbin, Shawn P., Dylan N. Dillaway, Eric L. Kruger, and Philip A. Townsend. 2012. “Leaf
700 Optical Properties Reflect Variation in Photosynthetic Metabolism and Its Sensitivity to
701 Temperature.” *Journal of Experimental Botany* 63 (1): 489–502.
702 <https://doi.org/10.1093/jxb/err294>.

703 Serbin, Shawn P., Jin Wu, Kim S. Ely, Eric L. Kruger, Philip A. Townsend, Ran Meng, Brett T.
704 Wolfe, Adam Chlus, Zhihui Wang, and Alistair Rogers. 2019. "From the Arctic to the
705 Tropics: Multibiome Prediction of Leaf Mass Per Area Using Leaf Reflectance." *New*
706 *Phytologist* 224 (4): 1557–68. <https://doi.org/10.1111/nph.16123>.

707 Shiklomanov, Alexey N., Ben Bond-Lamberty, Jeff W. Atkins, and Christopher M. Gough. 2020.
708 "Structure and Parameter Uncertainty in Centennial Projections of Forest Community
709 Structure and Carbon Cycling." *Global Change Biology* 26 (11): 6080–96.
710 <https://doi.org/10.1111/gcb.15164>.

711 Shiklomanov, Alexey N., Elizabeth M. Cowdery, Michael Bahn, Chaeho Byun, Steven Jansen,
712 Koen Kramer, Vanessa Minden, et al. 2020. "Does the Leaf Economic Spectrum Hold Within
713 Plant Functional Types? A Bayesian Multivariate Trait Meta-Analysis." *Ecological*
714 *Applications* 30 (3). <https://doi.org/10.1002/eap.2064>.

715 Simkin, Andrew J. 2021. "Carotenoids and Apocarotenoids in Planta: Their Role in Plant
716 Development, Contribution to the Flavour and Aroma of Fruits and Flowers, and Their
717 Nutraceutical Benefits." *Plants* 10 (11): 2321.
718 <https://doi.org/10.3390/plants10112321>.

719 Singh, Aditya, Shawn P. Serbin, Brenden E. McNeil, Clayton C. Kingdon, and Philip A.
720 Townsend. 2015. "Imaging Spectroscopy Algorithms for Mapping Canopy Foliar Chemical
721 and Morphological Traits and Their Uncertainties." *Ecological Applications* 25 (8): 2180–97.
722 <https://doi.org/10.1890/14-2098.1>.

723 Stan Development Team. 2018. "Stan Modeling Language Users Guide and Reference Manual,
724 Version 2.18. 0."

725 Sun, Tianhu, Sombir Rao, Xuesong Zhou, and Li Li. 2022. "Plant Carotenoids: Recent Advances
726 and Future Perspectives." *Molecular Horticulture* 2 (1): 3.
727 <https://doi.org/10.1186/s43897-022-00023-2>.

728 Thompson, David R., Vijay Natraj, Robert O. Green, Mark C. Helmlinger, Bo-Cai Gao, and
729 Michael L. Eastwood. 2018. "Optimal Estimation for Imaging Spectrometer Atmospheric
730 Correction." *Remote Sensing of Environment* 216 (October): 355–73.

731 <https://doi.org/10.1016/j.rse.2018.07.003>.

732 Ustin, Susan L., and Stéphane Jacquemoud. 2020. “How the Optical Properties of Leaves Modify
733 the Absorption and Scattering of Energy and Enhance Leaf Functionality.” In, edited by
734 Jeannine Cavender-Bares, John A. Gamon, and Philip A. Townsend, 349–84. Cham: Springer
735 International Publishing. https://doi.org/10.1007/978-3-030-33157-3_14.

736 Verrelst, Jochem, Zbyněk Malenovský, Christiaan Van der Tol, Gustau Camps-Valls,
737 Jean-Philippe Gastellu-Etchegorry, Philip Lewis, Peter North, and Jose Moreno. 2019.
738 “Quantifying Vegetation Biophysical Variables from Imaging Spectroscopy Data: A Review
739 on Retrieval Methods.” *Surveys in Geophysics* 40 (3): 589–629.
740 <https://doi.org/10.1007/s10712-018-9478-y>.

741 Violle, Cyrille, Marie-Laure Navas, Denis Vile, Elena Kazakou, Claire Fortunel, Irène Hummel,
742 and Eric Garnier. 2007. “Let the Concept of Trait Be Functional!” *Oikos* 116 (5): 882–92.
743 <https://doi.org/10.1111/j.0030-1299.2007.15559.x>.

744 Wang, Zhihui, Philip A. Townsend, Anna K. Schweiger, John J. Couture, Aditya Singh, Sarah E.
745 Hobbie, and Jeannine Cavender-Bares. 2019. “Mapping Foliar Functional Traits and Their
746 Uncertainties Across Three Years in a Grassland Experiment.” *Remote Sensing of
747 Environment* 221 (February): 405–16. <https://doi.org/10.1016/j.rse.2018.11.016>.

748 Wold, S., A. Ruhe, H. Wold, and W. J. Dunn, III. 1984. “The Collinearity Problem in Linear
749 Regression. The Partial Least Squares (PLS) Approach to Generalized Inverses.” *SIAM
750 Journal on Scientific and Statistical Computing* 5 (3): 735–43.
751 <https://doi.org/10.1137/0905052>.

752 Wright, Ian J., Peter B. Reich, Johannes H. C. Cornelissen, Daniel S. Falster, Philip K. Groom,
753 Kouki Hikosaka, William Lee, et al. 2005. “Modulation of Leaf Economic Traits and Trait
754 Relationships by Climate.” *Global Ecology and Biogeography* 14 (5): 411–21.
755 <https://doi.org/10.1111/j.1466-822x.2005.00172.x>.

756 Wullschleger, Stan D., Howard E. Epstein, Elgene O. Box, Eugénie S. Euskirchen, Santonu
757 Goswami, Colleen M. Iversen, Jens Kattge, Richard J. Norby, Peter M. van Bodegom, and
758 Xiaofeng Xu. 2014. “Plant Functional Types in Earth System Models: Past Experiences and

759 Future Directions for Application of Dynamic Vegetation Models in High-Latitude
760 Ecosystems.” *Annals of Botany* 114 (1): 1–16. <https://doi.org/10.1093/aob/mcu077>.
761 Xu, Chonggang, Rosie Fisher, Stan D. Wullschleger, Cathy J. Wilson, Michael Cai, and Nate G.
762 McDowell. 2012. “Toward a Mechanistic Modeling of Nitrogen Limitation on Vegetation
763 Dynamics.” *PLOS ONE* 7 (5): e37914.
764 <https://doi.org/10.1371/journal.pone.0037914>.